An Assessment of Improvements in Global Monsoon Precipitation Simulation in FGOALS-s2

ZHANG Lixia* and ZHOU Tianjun

State Key Laboratory of Numerical Modeling for Atmospheric Sciences and Geophysical Fluid Dynamics,

Institute of Atmospheric Physics, Chinese Academy of Sciences, Beijing 100029

ABSTRACT

The performance of Version 2 of the Flexible Global Ocean–Atmosphere–Land System model (FGOALS-s2) in simulating global monsoon precipitation (GMP) was evaluated. Compared with FGOALS-s1, higher skill in simulating the annual modes of climatological tropical precipitation and interannual variations of GMP are seen in FGOALS-s2. The simulated domains of the northwestern Pacific monsoon (NWPM) and North American monsoon are smaller than in FGOALS-s1. The main deficiency of FGOALS-s2 is that the NWPM has a weaker monsoon mode and stronger negative pattern in spring–fall asymmetric mode. The smaller NWPM domain in FGOALS-s2 is due to its simulated colder SST over the western Pacific warm pool. The relationship between ENSO and GMP is simulated reasonably by FGOALS-s2. However, the simulated precipitation anomaly over the South African monsoon region–South Indian Ocean during La Niña years is opposite to the observation. This results mainly from weaker warm SST anomaly over the maritime continent during La Niña years, leading to stronger upper-troposphere (lower-troposphere) divergence (convergence) over the Indian Ocean, and artificial vertical ascent (descent) over the Southwest Indian Ocean (South African monsoon region), inducing local excessive (deficient) rainfall. Comparison between the historical and pre-industrial simulations indicated that global land monsoon precipitation changes from 1901 to the 1970s were caused by internal variation of climate system. External forcing may have contributed to the increasing trend of the Australian monsoon since the 1980s. Finally, it shows that global warming could enhance GMP, especially over the northern hemispheric ocean monsoon and southern hemispheric land monsoon.

Key words: global monsoon precipitation, climate model, annual mode, climate change

Citation: Zhang, L. X., and T. J. Zhou, 2014: An assessment of improvements in global monsoon precipitation simulation in FGOALS-s2. *Adv. Atmos. Sci.*, **31**(1), 165–178, doi: 10.1007/s00376-013-2164-6.

1. Introduction

The global monsoon system is a persistent global-scale overturning of the atmosphere that varies with the time of year (Trenberth et al., 2000). It is a forced response of the coupled climate system to annual variation in solar forcing (Wang and Ding, 2008). Monsoon precipitation imposes great impacts on around two-thirds of the world's population, and thus observational and simulation studies on changes in global monsoon precipitation (GMP) are of great social and scientific importance.

The topic of GMP change has received a great deal of recent attention from the scientific community. For example, in terms of its climatology, Wang and Ding (2008) documented that the global monsoon can be represented by two annual multivariable EOF (MV-EOF) modes (the "monsoon mode" and "spring–fall asymmetric mode") of climatological monthly mean precipitation and low-level wind. Over the last 56 years, global land monsoon precipitation has undergone an overall weakening tendency (Wang and Ding, 2006), manifested in a combination of monsoon area and precipitation intensity changes (Zhou et al., 2008a). A recent assessment of global land monsoon precipitation during 1901–2001 showed that the decreasing trend is only significant for the last 50 years of that period, with an increasing trend found for the first 50 years of the 20th century (Zhang and Zhou, 2011). GMP enhanced during the period 1979–2008, originating primarily from an enhanced east–west thermal contrast in the Pacific Ocean and hemispherical thermal contrast (Wang et al., 2011).

Climate system models are useful tools in global monsoon studies. Based on an Atmospheric General Circulation Model (AGCM) driven by historical SST, Zhou et al. (2008b) revealed the forcing role of tropical SST on the decreasing trend of GMP since 1950. Meanwhile, examination of 21 coupled global climate models that participated in Phase 3 of the Coupled Model Intercomparison Project (CMIP3) showed that external volcanic forcings may play an important role in the decreasing trend of northern hemispheric land

---

* Corresponding author: ZHANG Lixia

  E-mail: lixiazhang@mail.iap.ac.cn

monsoon precipitation over the latter half of the 20th century (Kim et al., 2008). Using outputs based on the IPCC A1B scenario, Wang et al. (2011) reported that the increasing trend of GMP since 1980 may partly be due to anthropogenic forcing. Furthermore, based on high-resolution AGCMs, Hsu et al. (2012) found that global warming can also greatly affect GMP intensity and area.

Recently, a new spectral version (Version 2) of the Flexible Global Ocean–Atmosphere–Land System (FGOALS-s2) model, which participated in the fifth IPCC Assessment Report (IPCC AR5), was developed by the State Key Laboratory of Numerical Modeling for Atmospheric Sciences and Geophysical Fluid Dynamics (LASG) at the Institute of Atmospheric Physics (IAP), Chinese Academy of Sciences. As has been reported, the previous version of the model (FGOALS-s1) shows relatively low skill in simulating the spring-fall asymmetric mode of tropical precipitation, mainly due to the wrong annual cycle of tropical SST (Zhang et al., 2010). The performance of FGOALS-s2 has improved in various facets, such as the annual cycle of tropical SST, ENSO (Bao et al., 2013), East Asian summer monsoon (Wang et al., 2012), tropical intraseasonal oscillation (Yang et al., 2012) and long-term stability of oceanic circulations (Lin et al., 2013). Considering its importance, it is also desirable to fully assess the ability of the current version of the model to simulate global monsoon. Thus, the main motivation of the present study is to examine whether FGOALS-s2 has improved in terms of GMP simulation compared to FGOALS-s1. The following questions will be addressed: (1) Does the model show improvement in simulating the annual modes of GMP? (2) How does the model simulate the interannual variation of GMP? (3) Is the change in global land monsoon precipitation over the 20th century due to internal variability of the coupled ocean–atmosphere–land system, or the response to external forcings?

The remainder of the paper is organized as follows. In section 2, the model, datasets and method are introduced. The simulated climatological mean, interannual variation and impact of external forcing on GMP are reported in section 3. And finally, section 4 provides a summary of the major findings.

2.   Model, data and method

2.1.   *Model*

FGOALS-s2 comprises four component models coupled together by a flux coupler module from NCAR (Collins et al., 2006). The atmospheric component is Version 2 of the Spectral Atmospheric Model of IAP LASG (SAMIL2), which has a horizontal resolution of about $2.81°$ (lon) $\times 1.66°$ (lat) and 26 levels in the vertical direction (Bao et al., 2013). The ocean component is Version 2 of the LASG IAP Common Ocean Model (LICOM2), which has a horizontal resolution of about $1° \times 1°$ in the extra-tropical zone and $0.5° \times 0.5°$ in the tropics, and 30 vertical levels (Liu et al., 2012; Lin et al., 2013). The land and ice components are Version 3 of

the Community Land Model (CLM3) (Oleson et al., 2004) and Version 5 of the Community Sea Ice Model (CSIM5) (Collins et al., 2006), respectively. A more detailed description of these models can be found in Bao et al. (2013).

The pre-industrial simulation of FGOALS-s2 was used in the present study to evaluate the performance of the model. To compare with the previous version of model, the fully coupled 50-yr run of FGOALS-s1 was also used. Details about FGOALS-s1 can be found in Zhou et al. (2005) and Zhang et al. (2010). In addition to examining the impact of external forcing on global monsoon land precipitation changes, the historical run, forced by historical external forcing, and the Representative Concentration Pathways scenario for 2006–2100 covering the range 8.5 W m^{-2} (hereafter RCP8.5) were employed. There were three ensemble members for both the historical and RCP8.5 simulation of FGOALS-s2. Only one member was used for the pre-industrial run of both FGOLAS-s1 and FGOALS-s2.

2.2.   *Observational dataset*

The datasets used to evaluate the model performance include: (1) Precipitation data from the Global Precipitation Climatology Project (GPCP) (Adler et al., 2003) and the CPC Merged Analysis of Precipitation (CMAP) project (Xie and Arkin, 1997). The ensemble mean of the two datasets were used. (2) SST data from the Met Office Hadley Center's sea ice and SST (HadISST) dataset (Rayner et al., 1996). (3) Atmospheric circulation reanalysis data from the National Centers for Environment Prediction–Department of Energy Atmospheric Model Intercomparison Project II (NCEP2) Reanalysis (Kanamitsu et al., 2002). All data covered the period 1979–2008. (4) Monthly precipitation data for the global land surface during 1901–2002 compiled by the Global Precipitation Climatology Centre (hereafter GPCC) (Schneider et al., 2008) and by the Climate Research Unit (CRU) for the period 1901–2002 (Mitchell and Jones, 2005). The ensemble mean of the two datasets was used.

2.3.   *Methodology*

Because monsoon is characterized by an annual reversal of precipitation and wind (Webster et al., 1998), the annual modes of tropical precipitation are valuable objective standards for gauging the performance of climate models in simulating the mean state (Wang and Ding, 2008). These modes are the "monsoon mode" and "spring–fall asymmetric mode", and reflect the impact of anti-symmetric solar radiation forcing and asymmetry of rainfall between spring and fall, respectively. More details about the two modes can be found in Wang and Ding (2008) and Zhang et al. (2010).

Based on the annual modes, the global monsoon domain was defined in terms of rainfall characteristics (wet summer vs. dry winter) (Wang and Ding, 2008). It was delineated by the monsoon precipitation index, i.e., precipitation annual range normalized by the annual mean precipitation. The annual range was May–September (MJJAS) minus November–March (NDJFM) in the Northern Hemisphere and NDJFM minus MJJAS in the Southern Hemisphere. The monsoon

domains were taken to be the areas where the annual range exceeded 300 mm (2 mm d^{-1}) and the monsoon precipitation index exceeded 0.5.

The NH-averaged JJA precipitation and SH-averaged DJF precipitation falling in the monsoon domain were used to measure the strength of the Northern Hemisphere (NH) and Southern Hemisphere (SH) summer monsoon precipitation (hereafter NHMI and SHMI, respectively). The sum of NHMI and SHMI was used to quantify the strength of global monsoon (GMI) (Wang and Ding, 2006).

The interannual variation of GMP is closely related to ENSO (Ropelewski and Halpert, 1988; Dai and Wigley, 2000; Zhou et al., 2008b; Wang et al., 2011). Since FGOALS-s2 shows strong ability in reproducing the spatial pattern of ENSO and the double spectral peaks at around four and six years (Bao et al., 2013), the relationship between ENSO and GMP was also evaluated in the present study. To evaluate the performance of FGOALS-s2 in sim-

ulating its interannual variability, singular value decomposition (SVD) was performed on the monsoon-year-average precipitation and the corresponding SST. The "monsoon-year" runs between 1 May and 30 April, which is suitable for global monsoon and ENSO evolution (Wang et al., 2011).

3. Results

Using the fully coupled pre-industrial (or control) simulation of FGOALS-s1 and FGOALS-s2, the performances of the two models in simulating the annual models of tropical precipitation and the global monsoon domain, as well as interannual variations of GMP, are examined and compared in sections 3.1 and 3.2, respectively. Meanwhile, the potential mechanisms for simulation bias in FGOALS-s2 are also discussed. Since climatological and interannual variations can be simulated well by FGOALS-s2, the effect of external forcing on global land monsoon precipitation changes during
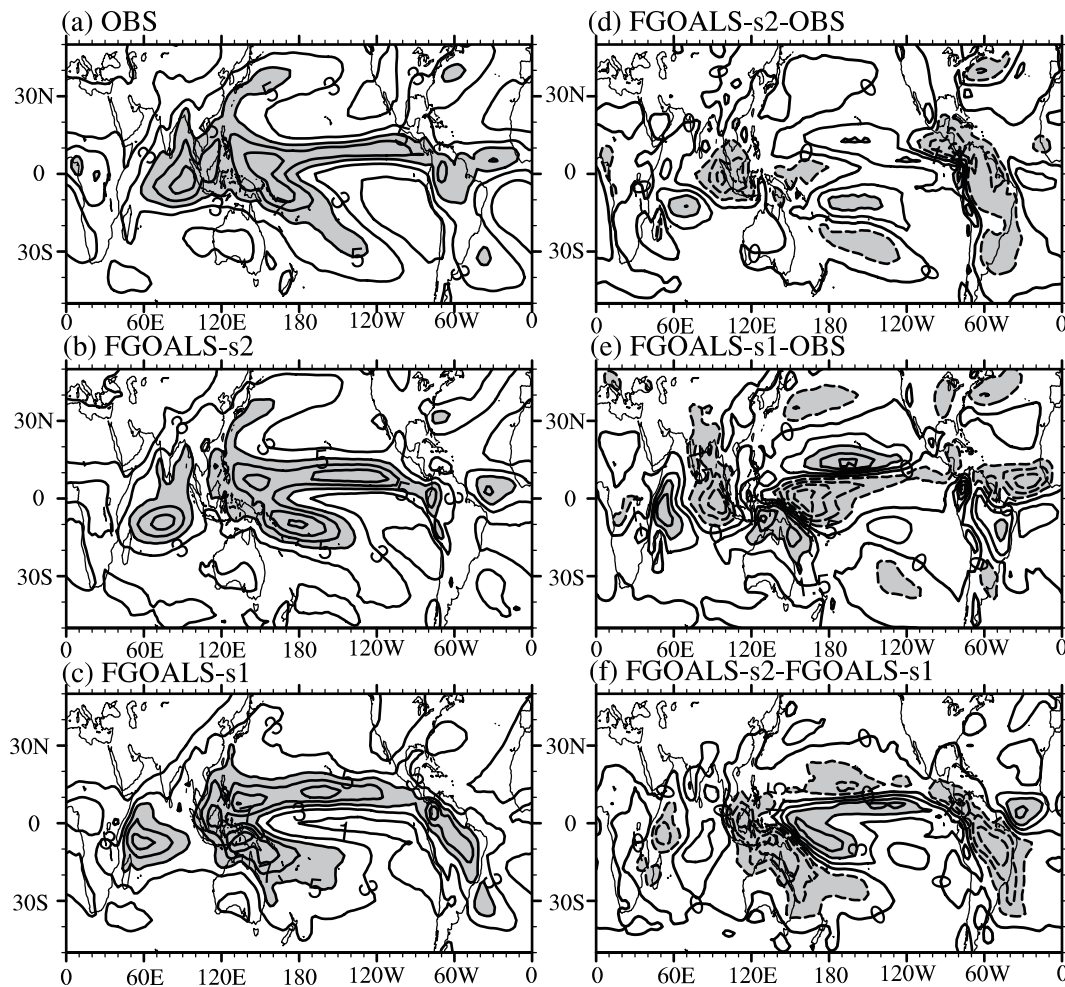

Fig. 1. The spatial patterns of climatological annual mean precipitation (units: mm d^{-1}) during 1990–99 derived from (a) observation; (b) pre-industrial simulation of FGOALS-s2; and (c) pre-industrial simulation of FGOALS-s1. (d) Difference between FGOALS-s2 and observation; (e) difference between FGOALS-s1 and observation; (f) difference between FGOALS-s2 and FGOALS-s1. The contour intervals for (a)–(c) and (d)–(f) are 3 mm d^{-1} and 1.5 mm d^{-1}, respectively. The precipitation intensities greater than 5 mm d^{-1} and 3 mm d^{-1} are shaded in (a)–(c) and (d)–(f), respectively.

1901–2001 is assessed using the pre-industrial and historical simulation results from FGOALS-s2.

3.1. *Annual modes of tropical precipitation*

The climatological means during 1979–2005 derived from observations and the historical simulations of the two versions of FGOALS-s are examined in this section. The geographical distributions of climatological annual mean precipitation according to observations and simulations are shown in Fig. 1. In the observation, major precipitation belts are located over the intertropical convergence zone (ITCZ), South Pacific convergence zone (SPCZ), western North Pacific Ocean, as well as over North Africa and South America adjacent to the ITCZ. The major precipitation belts are reproduced well by FGOALS-s2 (Fig. 1b). However, biases are also evident (Fig. 1d). The precipitation over the subtropical Pacific Ocean and South Indian Ocean is overestimated by FGOALS-s2, with the largest bias being greater than 3 mm d^{-1}. The excessive simulated precipitation in the equatorial northern Pacific is associated with the northward shift of the ITCZ in FGOALS-s2. Underestimated precipitation is seen over the warm pool region and South American monsoon, with the largest bias being -4 mm d^{-1}. The bias over East Asia is relatively small—less than 1 mm d^{-1} — indicating a good performance over that region.

Compared with FGOALS-s1 (Fig. 1c), the simulation of precipitation has improved in FGOALS-s2. The predicted pattern correlation coefficient (PCC) and root mean square error (RMSE) between FGOALS-s1 and the observation are 0.81 and 1.26 mm d^{-1}, respectively, while in FGOALS-s1 they are 0.72 and 1.61 mm d^{-1}, respectively. The excessive rainfall over Australia and the North Pacific (less simulated rainfall over India and the equatorial western Pacific) in FGOALS-s1 is greatly reduced (enhanced) in FGOALS-s2. An improvement over the Indian Ocean is not obvious (Figs. 1d–f). The PCC and RMSE between simulations and observations in different seasons are shown in Table 1. The PCC (RMSE) of FGOALS-s2 is higher (smaller) than that of FGOALS-s1 in all seasons, suggesting an improvement of FGOALS-s2 in terms of precipitation spatial distribution and intensity.

MV-EOF analysis was performed on the observed and simulated climatological monthly mean precipitation and wind at 850 hPa. The observed and simulated principal component time series of the first two leading MV-EOF modes are shown in Fig. 2. In the observation, the PC1 (PC2) reaches

Table 1. The PCCs and RMSEs between observations and simulations of FGOALS-s1 and FGOALS-s2 in different seasons. The units of RMSE are mm d^{-1}.

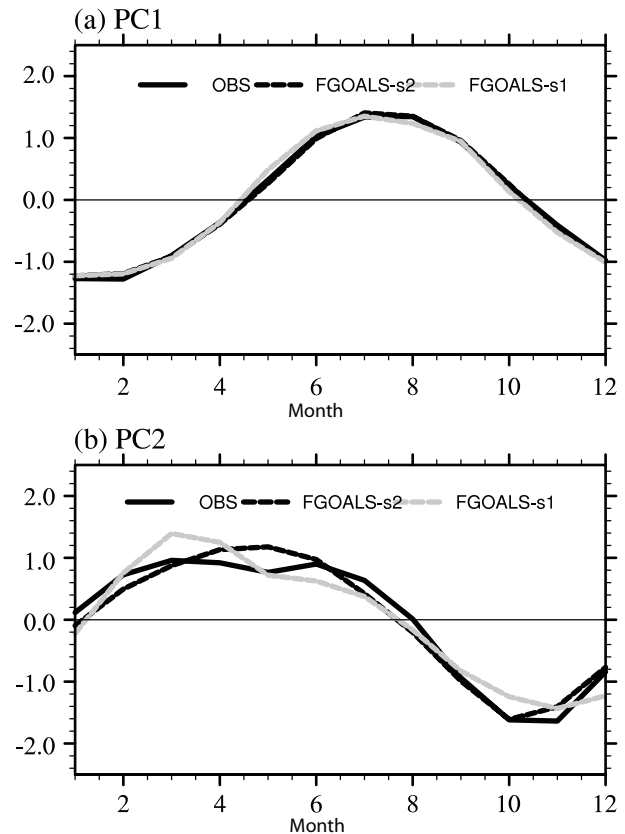|	PCC		RMSE	
	FGOALS-s1	FGOALS-s2	FGOALS-s1	FGOALS-s2
MAM	0.54	0.75	2.28	1.53
JJA	0.63	0.77	2.24	1.79
SON	0.75	0.79	1.69	1.51
DJF	0.72	0.83	2.13	1.43

Fig. 2. The principal component time series of the first two leading MV-EOF modes of climatological monthly precipitation and wind at 850 hPa derived from observation (black line), pre-industrial simulation of FGOALS-s2 (black dash line) and FGOALS-s1 (gray dash line): (a) PC1; (b) PC2.

its maximum in boreal summer (spring) and minimum in boreal winter (fall), and accounts for 71% (13%) of the total variance. These characteristics of the temporal evolution are simulated well by FGOALS-s2 and FGOALS-s1. The simulated PC1 and PC2 by FGOALS-s2 (FGOALS-s1) accounts for 67% (65%) and 18% (15%) of the total variance, respectively. The correlation coefficients of PC1 simulated by both versions with the observation are 1.0. The simulation of PC2 is improved by FGOALS-s2, with the correlation coefficient of PC2 becoming 0.98 from 0.96 in FGOALS-s1.

The observed and simulated spatial patterns of the first MV-EOF modes (monsoon modes) are shown in Fig. 3. The observed monsoon mode shows an anti-symmetric pattern about the Equator, i.e., the positive precipitation anomalies in East Asia, North America and North Africa, and the negative precipitation anomalies in South Africa, Australia and South America (Fig. 3a). The anti-symmetric pattern of the monsoon mode can be reproduced well by FGOALS-s2 (PCC = 0.78, RMSE = 0.80 mm d^{-1}), and has a higher skill than FGOALS-s1 (PCC = 0.64, RMSE = 1.11 mm d^{-1}). The simulated mode over the northwestern Pacific and North America is 3 mm d^{-1} weaker than the observation. The negative pattern over the Southwest Pacific Ocean is not reproduced by FGOALS-s2. Meanwhile, the simulated monsoon mode
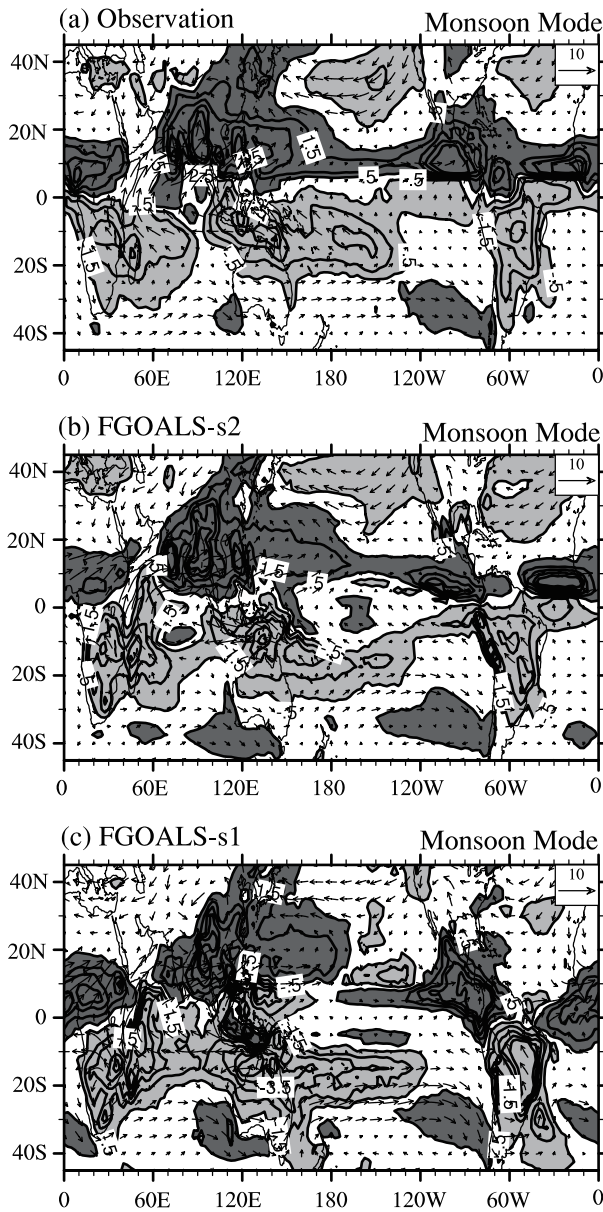
Fig. 3. The first MV-EOF mode of tropical precipitation (units: mm d^{-1}) and wind at 850 hPa (units: m s^{-1}) derived from (a) observation; (b) pre-industrial simulation of FGOALS-s2; and (c) pre-industrial simulation of FGOALS-s1. The contour intervals are 1 mm d^{-1}. The dark shaded areas are positive, while the light shaded areas are negative.

strength over South Africa is 2 mm d^{-1} stronger than the observation.

The intensity of the monsoon mode is overestimated by FGOALS-s1 (Fig. 3c) (Zhang et al., 2010). The monsoon mode strength in FGOALS-s1 is greater than that in FGOALS-s2, especially over the southern hemispheric monsoon region. The positive pattern over northern India monsoon is also well simulated by FGOALS-s2, but the positive pattern over the northeastern Pacific Ocean fails to be simulated by FGOALS-s1.

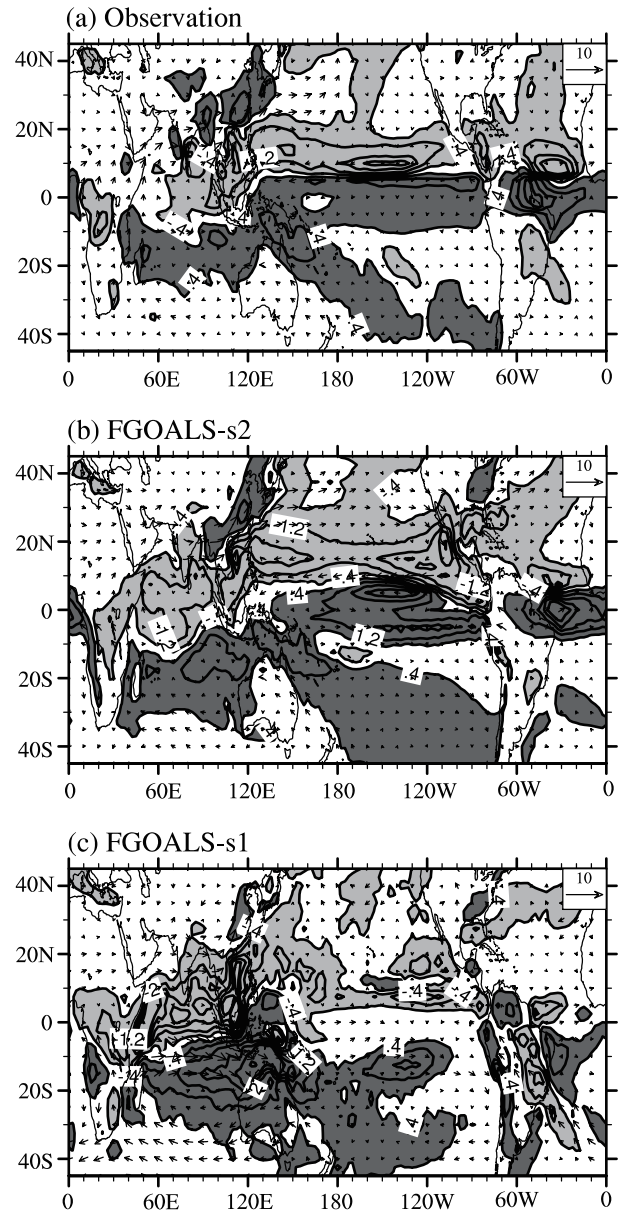The second annual mode—the "spring–fall asymmetric

Fig. 4. The same as Fig. 3, but for the second MV-EOF mode, i.e., spring–fall asymmetric mode. The contour intervals are 0.8 mm d^{-1}.

mode"—is shown in Fig. 4. In the observation, a negative pattern is seen mostly over the northern hemispheric ocean, while a positive pattern is seen over the Asian continent and southern hemispheric ocean. The positive pattern over South China is related to the first rainy season there. The main features of the second annual cycle mode are captured by FGOALS-s2, albeit with an overestimated strength of negative (positive) pattern over the northwestern Pacific and East Pacific (central equatorial Pacific) Ocean.

Compared with FGOALS-s1, the spring–fall asymmetric mode is greatly improved in FOGLAS-s2. The PCC and RMSE are 0.70 and 0.57 mm d^{-1}, respectively. In FGOALS-s1, these values are 0.57 and 0.82 mm d^{-1}, respectively. The improvement is mainly seen from the time of the first rainy

season in South China, with a more reasonable precipitation anomaly over the tropical Indian Ocean, as well as the equatorial Pacific and North Atlantic oceans. The improvement of the spring–fall asymmetric mode is related to reasonable simulation of the tropical SST annual cycle (not shown) (see Bao et al., 2013).

According to the definition of the monsoon domain proposed by (Wang and Ding, 2008), the distributions of precipitation annual range and the monsoon domain were obtained and are shown in Fig. 5. The major monsoon domains in FGOALS-s2 (Fig. 5b) are reproduced realistically (Fig. 5a), including the Asian–Australian monsoon, North and South African monsoon, and the North and South American monsoon. The largest deficiency of FGOALS-s2 is that it fails
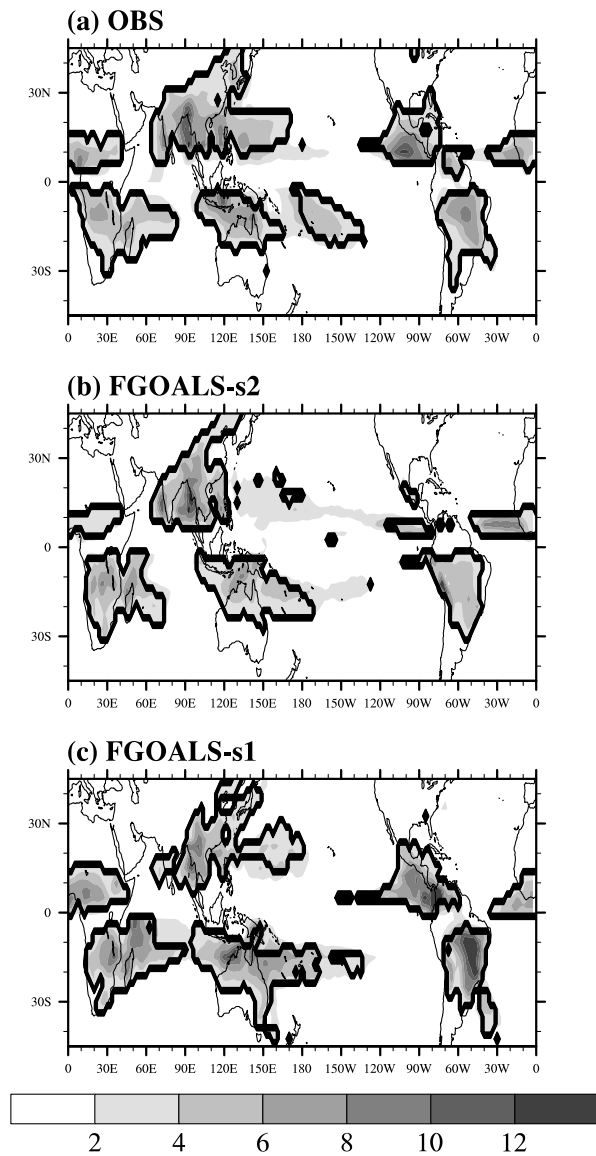
to simulate the northwestern Pacific monsoon (NWPM) domain, which is caused by the small precipitation contrast between boreal summer and winter (seen from the small value of annual range). The Asian monsoon and North American monsoon domains of FGOALS-s2 are smaller than those
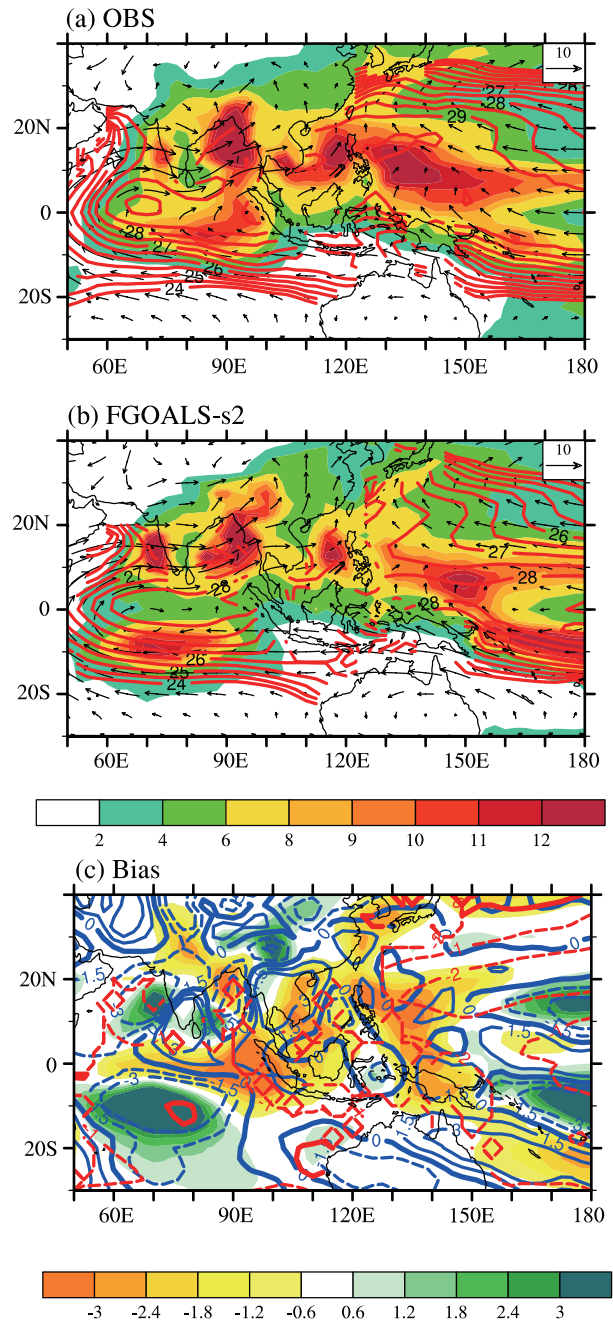

Fig. 5. The observed and simulated annual range of precipitation (shaded; units: mm d^{-1}) and global monsoon domain (contour) for (a) observation; (b) pre-industrial simulation of FGOALS-s2; and (c) pre-industrial simulation of FGOALS-s1.

Fig. 6. The climatological boreal summer mean (JJAS) precipitation (shaded; units: mm d^{-1}), wind at 850 hPa (vector; units: m s^{-1}) and SST (red lines; units: °C) derived from (a) observation and (b) pre-industrial simulation of FGOALS-s2. (c) Difference between (b) and (a). The blue lines in (c) are the simulation bias of vertical motion at 500 hPa (units: 10^{-2} hPa s^{-1}). The contour intervals for SST and vertical motion are 1°C and 1.5 × 10^{-2} hPa s^{-1}.
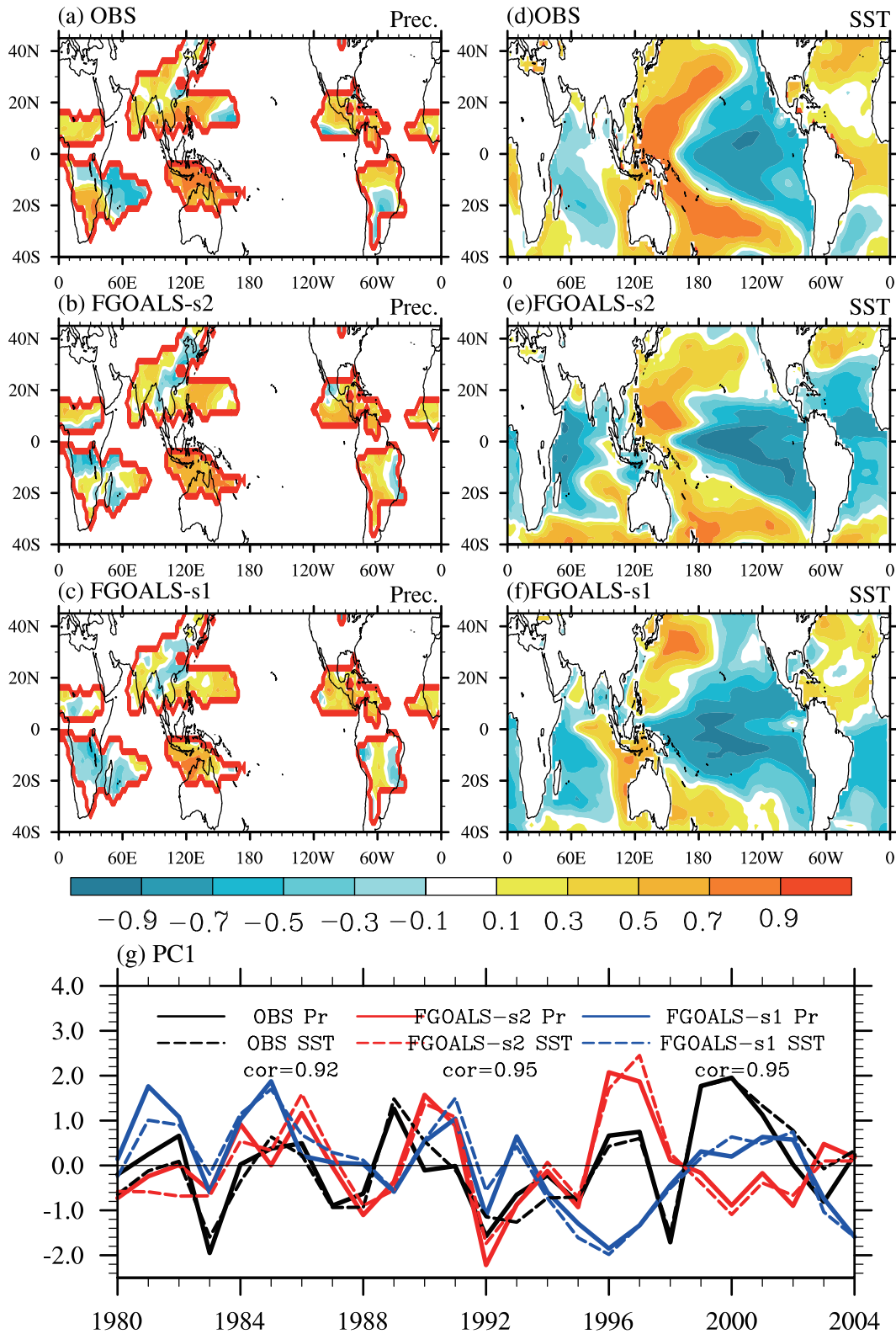
Fig. 7. The observed and simulated first leading mode of monsoon-year mean precipitation in global monsoon domains and the corresponding global SST derived from SVD analysis: (a) and (d) are the observed spatial patterns of monsoon precipitation and SST, respectively; (b) and (e) are the same as (a) and (d), but for pre-industrial simulation of FGOALS-s2; (c) and (f) are for pre-industrial simulation of FGOALS-s1; (g) is the corresponding time expansion coefficient in observations and simulations, respectively. The solid (dashed) lines depict the time series of precipitation (SST). The numbers in (g) show the correlation coefficients between precipitation and SST.

in the observation, while the Australian monsoon domain is larger. Compared with FGOALS-s1, the Indian monsoon and Australian monsoon are better simulated by FGOALS-s2, but the simulation domains of the NWPM and North American monsoon are much smaller than those in FGOALS-s1, although the NWPM domain in FGOALS-s1 is also smaller than in the observation.

To find out what causes the small rainfall contrast between boreal summer and winter over the NWPM in FGOALS-s2, the climatological summer (June to September) and winter (December to the following March) mean rainfall were examined. The results showed that the less simulated rainfall in boreal summer induces the abovementioned small rainfall contrast.

The climatological boreal summer mean precipitation, low-level wind and SST are shown in Fig. 6. In the observation, rainfall centers are seen from the NWPM to the Indian monsoon region, with the precipitation center of the NWPM reaching 20°N. The precipitation pattern can be reasonably simulated by FGOALS-s2, but with underestimated rainfall over the NWPM, which only reaches 10°N (Fig. 6b), inducing a small summer and winter rainfall contrast. The rainfall over the NWPM is located in the north of the warm pool and is related with the strong convection (seen from convergence wind at 850 hPa) induced by local warm SST, which can be seen from the spatial pattern of SST (> 29°C) in the observation (Fig. 6a). In FGOALS-s2 (Fig. 6b), the SST over

the northwestern Pacific warm pool is 2°C colder than the observation, with the warmest SST being 27°C. The colder SST suppresses convection (divergence wind at 850 hPa) and induces less local rainfall (Fig. 6c), leading to less rainfall contrast between summer and winter. The circulation bias of FGOALS-s1 was also examined (not shown). This showed that the SST of the warm pool over the western Pacific is also cooler than the observation, which induces weaker summer precipitation over the NWPM of FGOALS-s1. The SST of the warm pool over the western Pacific in FGOALS-s1 is about 1°C cooler than that in FGOALS-s2 and results in its much weaker summer precipitation over the southern part of the NWPM.

3.2. *Interannual variation of GMP*

The first SVD mode (SVD1) between GMP and SST in observations and simulations are shown in Fig. 7. The observed SVD1 explains 54% of the total covariance. The temporal correlation coefficient between precipitation and SST is 0.92—statistically significant at the 5% level. The spatial pattern of precipitation shows increased rainfall in nearly all regional monsoons, except for the southwestern Indian Ocean and the southern part of the South American monsoon (Fig. 7a). This concurs with significant cooling over the equatorial Pacific Ocean, indicating GMP tends to increase during La Niña years or decrease during El Niño years (Fig. 7d).

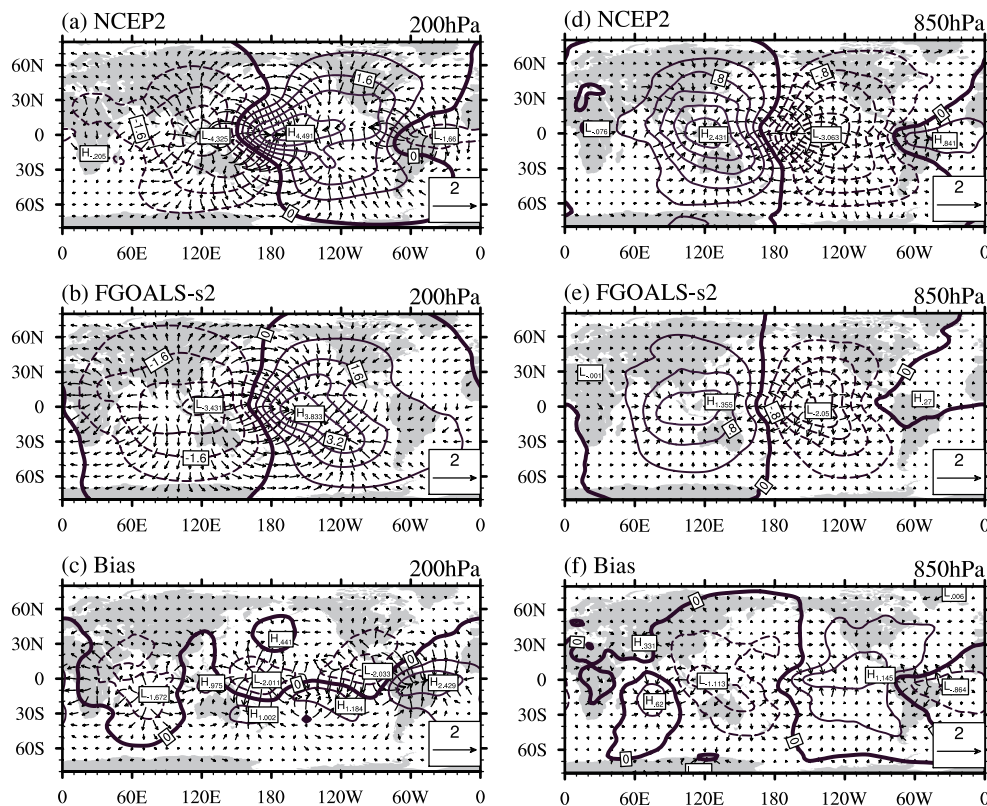The SVD1 modes of GMP and SST in FGOALS-s1 and

Fig. 8. Composite annual mean velocity potential anomalies (contour; units: 10^6 m^2 s^{-1}) and divergence wind (vector; units: m s^{-1}) at 200 hPa during ENSO years at 200 hPa for (a) the NCEP–NCAR reanalysis and (b) pre-industrial simulation of FGOALS-s2. (d) Difference between FGOALS-s2 and NCEP-NCAR reanalysis. (d)–(f) The same as (a)–(c), but for 850 hPa.

FGOALS-s2 both indicate the relationship between ENSO and GMP (Figs. 7b, c and Figs. 7e, f). The SVD1 of FGOALS-s1 and FGOALS-s2 explains 39% and 56% of the total covariance, respectively. The explained variance of FGOALS-s2 is much closer to that of the observation. The correlation coefficients between simulated rainfall and SST are both 0.95 in the two versions of FGOALS-s—also statistically significant at the 5% level.

The simulation biases are evident, especially over the South African monsoon–Southwest Indian Ocean and North China. In the observation, the precipitation over the South African monsoon–Southwest Indian Ocean exhibits a west positive–east negative dipole pattern, while North China rainfall is nearly all above normal. In FGOALS-s2 and FGOALS-s1, a west negative–east positive dipole pattern (negative precipitation anomaly) is obvious over the South African monsoon–Southwest Indian Ocean (North China). The simulated SST anomalies (SSTAs) over the tropical Pacific Ocean of SVD1 are both stronger and extended farther west than in the observation in the two versions of FGOALS-s, especially over the tropical Indian Ocean (Figs. 7e and f). Compared with FGOALS-s1, the western-extended cold SSTA over the Pacific Ocean is improved in FGOALS-s2. However, a cold SSTA exists over the North Atlantic Ocean in FGOALS-s2, which is warm in FGOALS-s1 and the observation.

Since the simulated precipitation bias during ENSO years over the South African monsoon–Southwest Indian Ocean are closely related with circulation anomalies, the composite divergence wind during ENSO years (difference between La Niña and El Niño) of FGOALS-s2 were investigated and the results are shown in Fig. 8. In the NCEP2 reanalysis, the upper-level (lower-level) convergences (divergences) over the eastern hemisphere are centered over the central Pacific Ocean during La Niña years. Meanwhile, the western hemisphere features a divergence (convergence) at the upper levels (lower levels), centered over the maritime continent. A weak anomalous convergence (divergence) dominates the Southwest Indian Ocean at 200 hPa (850 hPa). The South African monsoon shows an opposite circulation anomaly to that over the Southwest Indian Ocean. This will suppress (enhance) the local vertical motion and thus reduce (increase) rainfall over the Southwest Indian Ocean (South African monsoon).

The circulation anomalies during ENSO years are reproduced well by FGOALS-s2. However, the simulated divergence wind at 200 hPa (850 hPa) in FGOALS-s2 is stronger (weaker) over the Indian Ocean and weaker (stronger) over the maritime continent than in the observation (Figs. 8c and f). This will enhance the local vertical motion and lead to heavier precipitation over the Southwest Indian Ocean. Over the South African monsoon, a weak divergence is seen in the lower troposphere, which is favorable for stronger monsoon rainfall. Therefore, the west negative–east positive dipole pattern over the South African monsoon–Southwest Indian Ocean is seen in FGOALS-s2. The divergent wind is mainly caused by the simulated SST bias of FGOALS-s2 during ENSO years. In FGOALS-s2, the cold SST anomalies in the central tropical Pacific Ocean during La Niña years are

about $10°$ westward compared to the observation, and the warm SST anomalies over the western Pacific are cooler than in the observation (Figs. 6d and e), leading to weaker anti-Walker circulation over the Indian Ocean. This will suppress the convection over the maritime continent and enhance the convection over the South Indian Ocean (Figs. 8c and f).

3.3. *Effect of external forcing on global land monsoon precipitation changes during* 1901–2001

The changes in global land monsoon precipitation for 1901–2001 have been well documented by Zhang and Zhou (2011). However, up to now, no effort has been made to examine the effect of external forcing on global land monsoon rainfall changes. The historical run and pre-industrial simulation (piControl) of FGOALS-s2 was used to address this question.

The observed and simulated 5-yr running mean time series of NHMI, SHMI and GMI are shown in Fig. 9. The standard deviations of observations are 0.24 mm d^{-1}, 0.32
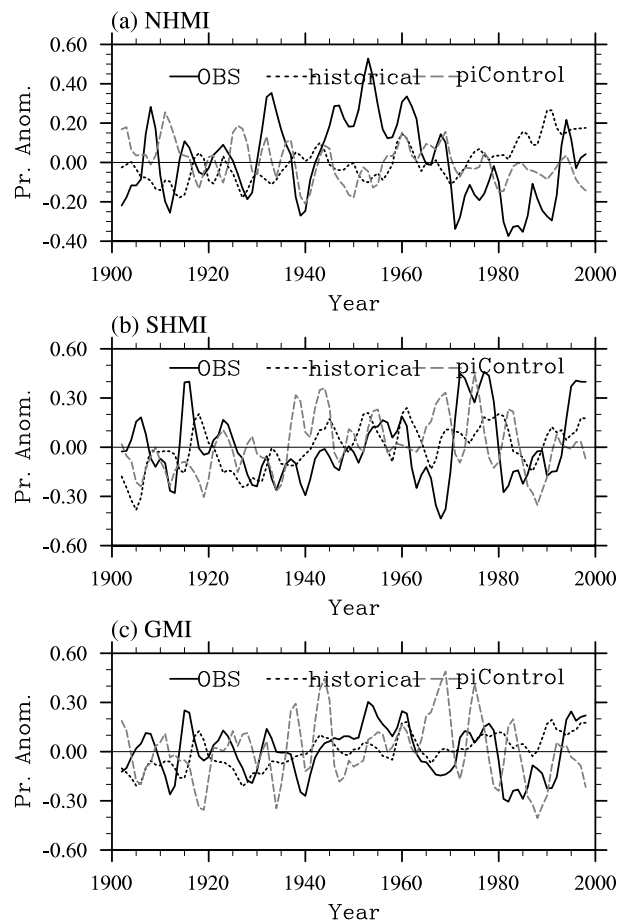

Fig. 9. The observed and simulated monsoon precipitation changes (5-yr running mean; units: mm d^{-1}) during 1900–2000 for (a) NH mean; (b) SH mean; and (c) global mean. The black, black dash and grey lines represent the observation, historical run of FGOALS-s2 and pre-industrial run of FGOALS-s2, respectively.

mm d^{-1} and 0.34 mm d^{-1} for GMI, NHMI and SHMI, respectively. Global and NH land monsoon precipitation (Figs. 9a and c) undergoes an upward trend from 1901 to the 1950s, followed by a downward trend from the 1950s to 1980s and a recovery since the 1980s. SH land monsoon precipitation has no significant trend.

The GMP and NH changes in piControl show evident interannual and interdecadal variation, and no significant trend in GMI and NHMI, as in the observation. In the historical simulation of FGOALS-s2, which considered the contribution of anthropogenic forcing (greenhouse gases and sulfate aerosols), the increasing (decreasing) trend between 1901 and the 1950s (since 1950s) could not be simulated. The observed recovery of monsoon precipitation in the NH since the 1980s is partly reproduced by the historical run of FGOALS-s2. The linear trends of monsoon precipitation for every 21-

yr running time series simulated by piControl and historical runs of FGOALS-s2 were examined. The linear trend [0.06 mm d^{-1} (10 yr)$^{-1}$] for 1980–2000 in the historical simulation fails within the bound of trends for every 21-yr in both piControl [0.10 mm d^{-1} (10 yr)$^{-1}$] and the historical run [0.14 mm d^{-1} (10 yr)$^{-1}$]. Although the observed increasing trend since the 1980s is partly produced by the historical simulation, it cannot determine whether or not it is caused by external or internal forcing.

In order to reveal the coherent pattern of global land monsoon precipitation changes, EOF analysis was performed on the precipitation annual range in the global land monsoon domain (Fig. 10). EOF1 accounts for 6.1% of the total variance in the observation. The majority of global land monsoon precipitation in the observed EOF1 shows coherent change. The corresponding PC also suggests an increasing trend during
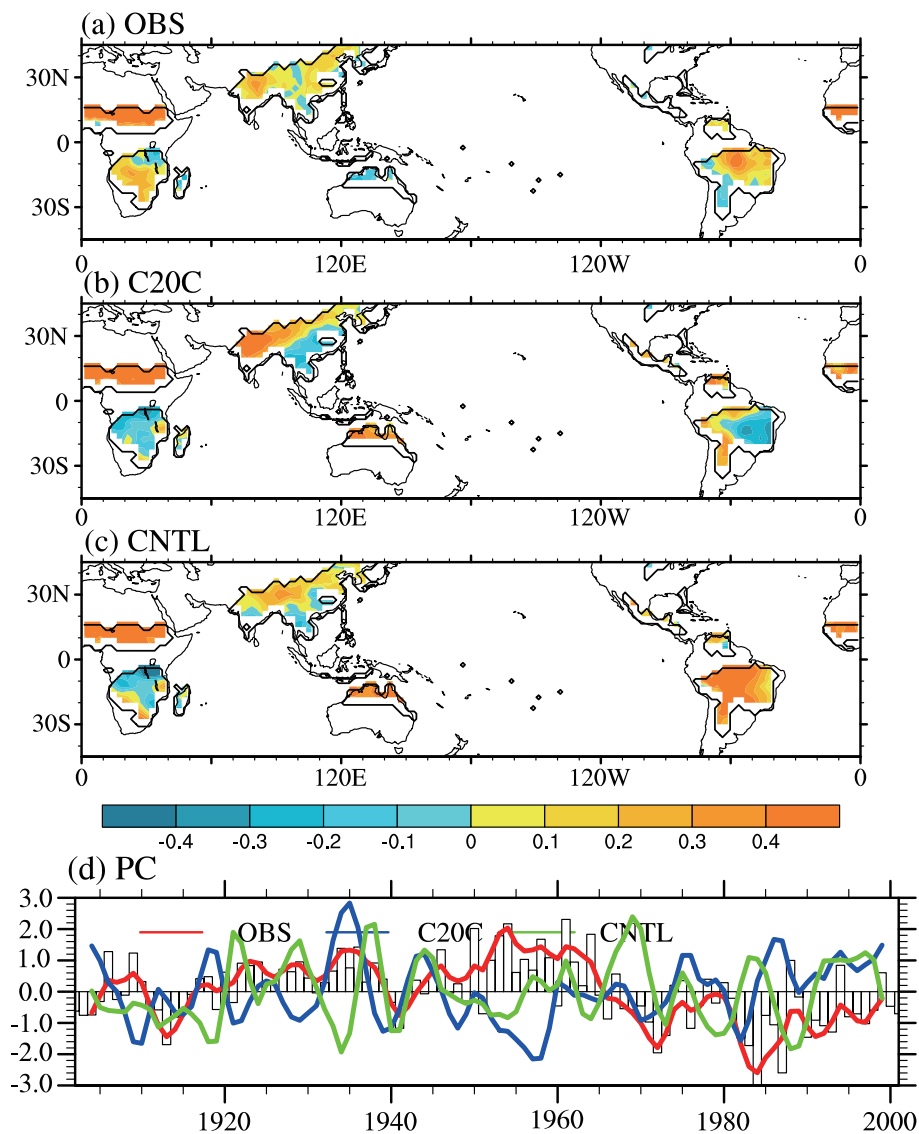

Fig. 10. The first EOF mode of global land monsoon precipitation for 1901–2001 for (a) observation; (b) historical run of FGOALS-s2; and (c) pre-industrial run of FGOALS-s2. (d) Corresponding principal component (5-yr running mean).

1901–1955, a decreasing trend since the 1950s, and a recovery since the 1980s. Both the historical and piControl simulation simulate the spatial pattern of EOF1 well, but with the largest deficiency over the East Asian monsoon, South American monsoon and Australian monsoon. The PC time serial from the historical simulation shows an increasing trend since the 1980s, as in the observation, which cannot be found in the piControl simulation. Neither the historical or piControl simulation can simulate the above normal precipitation during the 1950s or the increasing tendency from 1901 to the 1950s.

To reveal the contribution of external forcing on the precipitation of each regional monsoon, the observed and simulated precipitation changes during local summer (i.e., JJAS in the NH and DJFM in the SH) in regional monsoons are shown in Fig. 11. In the observation, the increasing trends from 1901 to the 1950s can be found in the North African and East Asian monsoon, while the decreasing trend since the 1950s is seen mainly in the North African and Indian monsoon regions. This has been well documented previously by Zhou et al. (2008b) and Zhang and Zhou (2011). For the

recovery of monsoon precipitation since 1980s, this can be found from the North African, East Asian, South African and Australian monsoons. The linear trend of the precipitation of each regional monsoon during 1981–2001 is shown in Table 2. Only the increasing trends in the North African monsoon [0.25 mm d^{-1} (10 yr)$^{-1}$] and East Asian monsoon [0.21 mm d^{-1} (10 yr)$^{-1}$] are statistically significant at the 5% level. The tendency of the Australian monsoon is the strongest [0.84 mm d^{-1} (10 yr)$^{-1}$], but does not exceed the 95% confidence level.

Neither the historical or piControl simulation is able to simulate the increasing trend from 1901 to the 1950s in the North African and Indian monsoon. This further indicates that precipitation changes for the first 50 years of the 20th century were a result of internal climate variation. Comparison between the historical and piControl simulation of FGOALS-s2 for the period since the 1980s shows that external forcing mainly contributes to the increased precipitation over the North African and Australian monsoons. For all the regional monsoon precipitation changes, only the increasing
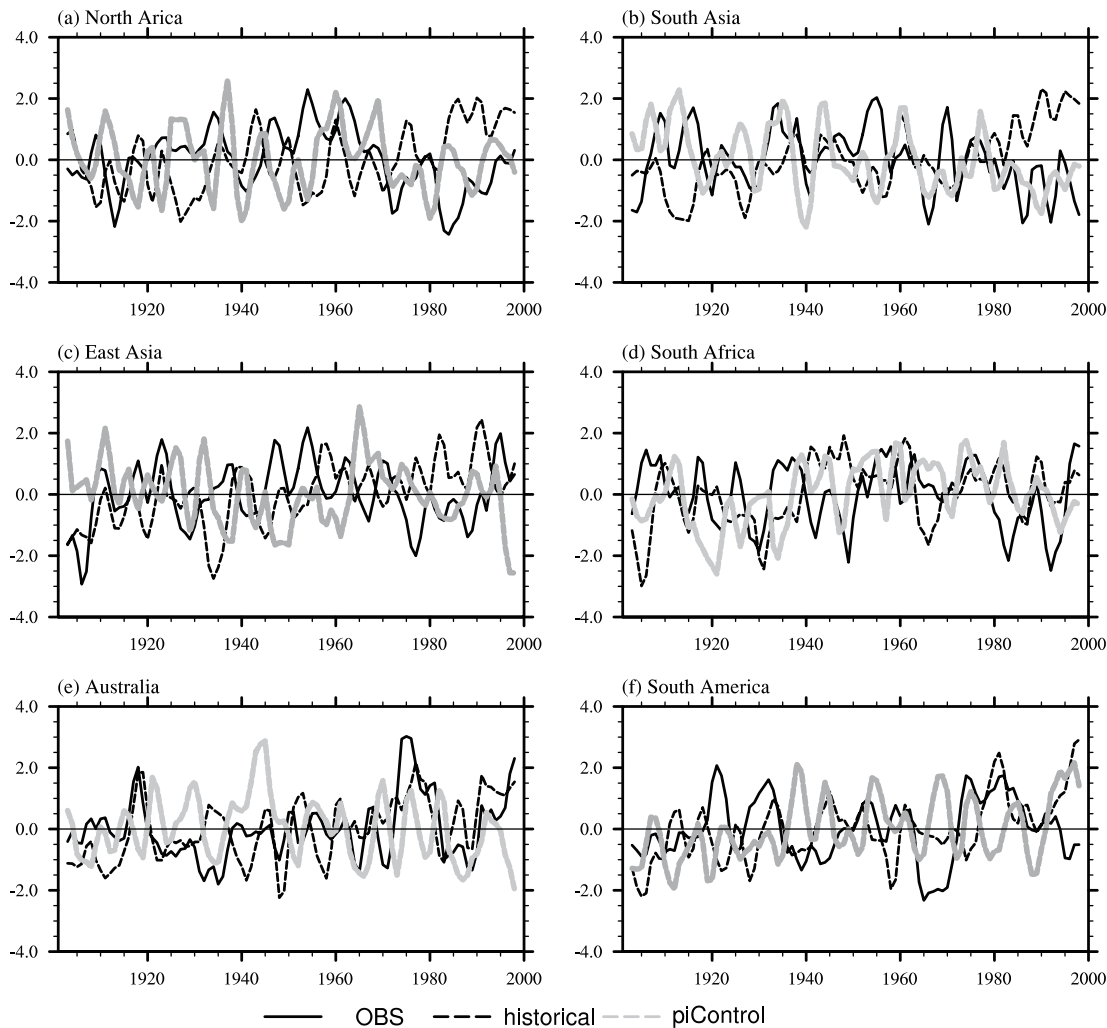

Fig. 11. The observed and simulated normalized land monsoon precipitation changes in each regional monsoon: (a) North African monsoon; (b) Indian monsoon; (c) East Asian monsoon; (d) South African monsoon; (e) Australian monsoon; and (f) South American monsoon.
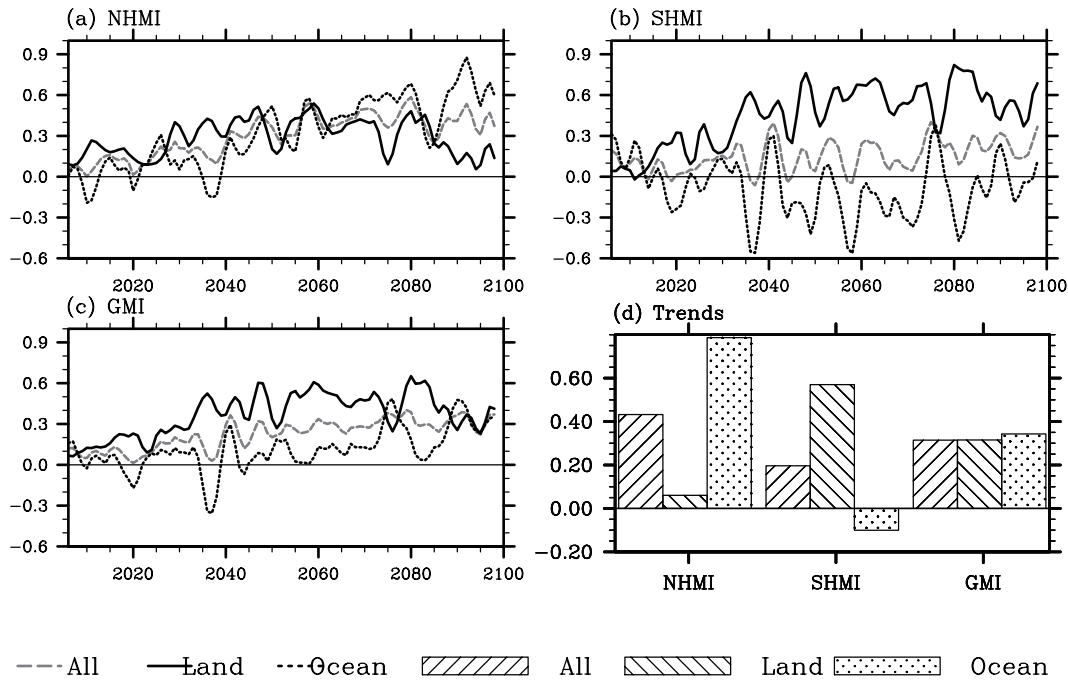
Fig. 12. The projected 5-yr running mean monsoon precipitation anomalies (relative to climatology of 1986–2005; units: mm d^{-1}) during 2006–2100 for (a) NHMI; (b) SHMI; and (c) GMI. (d) Linear trend of monsoon precipitation of each region for 2006–2100 [units: mm d^{-1} (100 yr)$^{-1}$]. The black, black dash and grey dash lines in (a)–(c) are precipitation indices of all monsoons, land monsoons and ocean monsoons, respectively.

Table 2. The linear trend [units: mm d^{-1} (10 yr)$^{-1}$] of the land monsoon precipitation of each region during 1980–2000. Values with asterisks are statistically significant at the 5% level according to the Student's t-test.

	Observation	Historical	piControl
North Africa	0.25*	0.03	−0.005
India	−0.14	0.29	0.07
East Asia	0.21*	−0.09	−0.09
South Africa	0.24	−0.02	−0.06
Australia	0.84	0.52*	−0.65
South America	−0.46*	0.14	0.12

tendency of the Australian monsoon [0.52 mm d^{-1} (10 yr)$^{-1}$] exceeds its largest trend [0.46 mm d^{-1} (10 yr)$^{-1}$] for every 21-yr running time series in the historical simulation. The impact on the Australian monsoon is the largest, which can also be seen from the difference between the trends for the period since the 1980s in the historical and piControl simulations, which is 0.52 mm d^{-1} (10 yr)$^{-1}$ in the historical simulation, while it is negative [−0.65 mm d^{-1} (10 yr)$^{-1}$] in piControl.

During the past 100 years, the Earth's climate has been dominated by a warming trend. It is useful to see whether global warming has any effect on GMP changes, and the monsoon precipitation indices simulated by FGOALS-s2 under the RCP8.5 emission scenario were thus examined and the results are shown in Fig. 12. Increasing trends from 2006 to 2100 can be seen from all the monsoon precipitation indices, except for that over the southern hemisphere oceanic

monsoon. GMP is predicted to increase under the RCP8.5 scenario, with the amplitude at 0.33 mm d^{-1} (100 yr)$^{-1}$. The increasing strengths for land monsoon precipitation [0.32 mm d^{-1} (100 yr)$^{-1}$] are close to those of ocean monsoon precipitation [0.34 mm d^{-1} (100 yr)$^{-1}$]. The northern hemispheric ocean monsoon precipitation might experience the strongest tendency, with a linear trend of 0.63 mm d^{-1} (100 yr)$^{-1}$ and statistically significant at the 5% level. The second strongest growing trend is seen for the southern hemispheric land monsoon rainfall — also statistically significant at the 5% level. The increase of GMP under a warming scenario is consistent with the findings of Wang et al. (2011) and Hsu et al. (2012), whose studies were based on the IPCC AR4 A1B scenario.

4. Summary

The performance of FGOALS-s2 in simulating GMP change was systematically evaluated. GMP is simulated well by FGOALS-s2, including its climatological mean and interannual variation. Comparison between FGOALS-s2 and its former version (FGOALS-s1) in simulating the annual cycle and interannual variation of GMP was also carried out. Furthermore, by comparing the historical simulation and preindustrial simulation of FGOALS-s2, the impact of external forcing on global land monsoon precipitation changes during the 20th century was assessed. The major conclusions can be summarized as follows.

(1) Compared with FGOALS-s1, the annual mean precipitation, monsoon mode and spring–fall asymmetric mode of climatological mean tropical precipitation and circulation

are improved by FGOALS-s2, especially for the spring–fall asymmetric mode. However, the simulation domains of the NWPM and North American monsoon are much smaller than in FGOALS-s1.The anti-symmetrical pattern of the monsoon mode is simulated realistically by FGOALS-s2, but with weaker magnitude over the northwestern Pacific and North America and stronger intensity over South Africa. For the spring–fall asymmetric mode, the negative pattern over the northern hemispheric ocean and positive pattern over the Asian continent and southern hemispheric ocean are also simulated reasonably, but with an overestimated negative (positive) pattern over the northwestern and eastern Pacific (central equatorial Pacific) oceans. The major global monsoon domains are simulated realistically by FGOALS-s2, while the northwestern Pacific monsoon fails to be captured, which is due to colder SST over the northwestern Pacific warm pool, leading to weaker convection and thereby less rainfall.

(2) The observed interannual variation of GMP is related with ENSO. GMP tends to increase in La Niña years or decrease in El Niño years. The relationship between ENSO and GMP is reproduced reasonably by FGOALS-s2, which shows a better performance than FGOALS-s1 in simulating SSTA over the tropical Pacific Ocean. However, the simulated precipitation anomaly over the South African monsoon–Southwest Indian Ocean in FGOALS-s2 is opposite to the observation. This largely results from the simulated weaker warm SST anomaly over the maritime continent during La Niña years, leading to the upper-troposphere (lower-troposphere) divergence (convergence) over the Indian Ocean being stronger than in the observation, and artificial vertical ascent (decent) over the Southwest Indian Ocean (South African monsoon), thereby inducing local excessive (deficient) rainfall.

(3) Global land monsoon precipitation shows an increasing trend from 1901 to the 1950s, followed by a decreasing tendency up to the 1980s, and a recovery after the 1980s. Comparison between the historical and piControl simulations indicated that global land monsoon precipitation changes from 1901 to the 1970s were mainly caused by internal variation of the climate system. The recovery of GMP since the 1980s is partly reproduced by the historical simulation of FGOALS-s2. However, it fails in the band of trends for every 21-yr running time series in both the piControl and historical run. Examination of each regional monsoon indicated that the impact of external forcing is important for the Australian monsoon. The simulation under the RCP8.5 emission scenario showed that global warming is likely to enhance GMP, especially over the northern hemispheric ocean monsoon regions and southern hemispheric land monsoon regions.

REFERENCES

Adler, R. F., and Coauthors, 2003: The version-2 global precipitation climatology project 11 (GPCP) monthly precipitation analysis (1979-present). *J. Hydrometeor.*, **4**, 1147–1167.

Bao, Q., G. X. Wu, Y. M. Liu, J. Yang, Z. Z. Wang, and T. J. Zhou, 2010: An introduction to the coupled model FGOALS1.1-s and its performance in East Asia. *Adv. Atmos. Sci.*, **27**(5), 1131–1142, doi: 10.1007/s00376-010-9177-1.

Bao, Q., and Coauthors, 2013: The flexible global ocean-atmosphere-land system model version: FGOALS-s2. *Adv. Atmos. Sci.*, **31**(2), doi: 10.1007/s00376-012-2113-9.

Collins, W. D., and Coauthors, 2006: The community climate system model version 3 (CCSM3). *J. Climate*, **19**, 2122–2143.

Dai, A., and T. Wigley, 2000: Global patterns of ENSO-induced precipitation. *Geophys. Res. Lett.*, **33**(9), 1283–1286.

Hsu, P. C., T. Li, J. Luo, H. Murakami, A. Kitoh, and M. Zhao, 2012: Increase of global monsoon area and precipitation under global warming: A robust signal? *Geophys. Res. Lett.*, **29**, L06701, doi: 10.1029/2012GL051037.

Kanamitsu, M., W. Ebisuzaki, J. Woollen, S.-K. Yang, J. J. Hnilo, M. Fiorino, and G. L. Potter, 2002: NCEP-DOE AMIP-II Reanalysis (R-2). *Bull. Amer. Meteor. Soc.*, **83**, 1631–1643.

Kim, H., B. Wang., and Q. Ding., 2008: Assessing the global monsoon simulated by the CMIP3 coupled climate models. *J. Climate*, **21**, 5271–5294.

Lin, P. F., Y. Q. Yu, and H. L. Liu, 2013: Long-term stability and oceanic mean state simulated by the coupled model FGOALS-s2. *Adv. Atmos. Sci.*, **30**(1), 175–192, doi: 10.1007/s00376-012-2042-7.

Liu, H., P. Lin, Y. Yu, and X. Zhang, 2012: The baseline evaluation of LASG/IAP climate system ocean model (LICOM) version 2.0. *Acta Meteorologica Sinica*, **26**(3), 318–329.

Mitchell, T., and P. Jones, 2005: An improved method of constructing a database of monthly climate observations and associated high-resolution grids. *Int. J. Climatol.*, **25**, 693–712.

Oleson, K. and Coauthors, 2004: Technique description of the Community Land Model (CLM). Tech. Rep. NCAR/TN-461+STR, National Center for Atmospheric Research, Boulder, CO, 174 pp.

Rayner, N. A., E. B. Horton, D. E. Parker, C. K. Folland, and R. B. Hackett, 1996: Version 2.2 of the global sea-ice and sea surface temperature dataset, 1903–1994. Climate Research Technical Note, No. 74, 1–21.

Ropelewski, C., and M. Halpert, 1988: Global and regional scale precipitation patterns associated with the El Nino-Southern Oscillation. *Mon. Wea. Rev.*, **115**(8), 1606–1626.

Schneider, U., T. Fuchs., A. Meyer-Christoffer, and B. Rudolf., 2008: Global precipitation analysis products of the GPCC. Global Precipitation Climatology Centre (GPCC), DWD, *Internet Publication*, 1–12.

Trenberth, K. E., D. P. Stepaniak, and J. M. Caron, 2000: The global monsoon as seen through the divergent atmospheric circulation. *J. Climate*, **13**, 3969–3993.

Wang, B., and Q. Ding, 2006: Changes in global monsoon precipitation over the past 56 years. *Geophys. Res. Lett.*, **33**, L06711, doi: 10.1029/2005GL025347.

Wang, B., and Q. Ding, 2008: The global monsoon: major modes of annual variation in Tropical precipitation and circulation. *Dyn. Atmos. Oceans*, **44**, 165–183.

Wang B., J. Liu, H. Kim, P. J. Webster, and S. Y. Yim, 2011: Recent change of the global monsoon precipitation (1979–

2008). *Climate Dyn.*, doi: 10.1007/s00382-011-1266-z.

Wang, J., Q. Bao, Y. Liu, G. Wu, B. He, and X. Wang, 2012: Performance of SAMIL on the global heating and the East Asian summer monsoon. *Chinese J. Atmos. Sci.*, **36**(1), 63–76. (in Chinese)

Webster, P., V. Magaña, T. Palmer, J. Shukla, R.Tomas, M. Yanai, and T. Yasunari, 1998: Monsoons: Processes, predictability and the prospects for prediction. *J. Geophys. Res.*, **103**, 14451–14510.

Xie, P., and P. A. Arkin, 1997: Global precipitation: A 17-year monthly analysis based on gauge observations, satellite estimates, and numerical model outputs. *Bull. Amer. Meteor. Soc.*, **78**, 2539–2558.

Yang, J., Q. Bao, X. C. Wang, and T. J. Zhou, 2012: The tropical intraseasonal oscillation in SAMIL coupled and uncoupled general circulation models. *Adv. Atmos. Sci.*, **29**(3), 529–543, doi: 10.1007/s00376-011-1087-3.

Zhang, L., and T. Zhou, 2011: An assessment of monsoon precipitation changes during 1901–2001. *Climate Dyn.*, **37**, 279–296, doi: 10.1007/s00382-011-0993-5.

Zhang, L., T. Zhou, B. Wu, and Q. Bao, 2010: The annual modes of tropical precipitation simulated by the LASG/IAP coupled ocean-atmosphere model FGOALS_s1.1. *Acta Meteorologica Sinica*, **24**(2), 189–202.

Zhou, T., R. Yu, Z. Wang, T. Wu, 2005: *Atmosphere Circulation Model SAMIL and the Fully Coupled Model FGOALS-s*. China Meteorological Press, Beijing, 288 pp. (in Chinese)

Zhou, T. J., R. Yu, H. Li, and B. Wang 2008a: Ocean forcing to changes in global monsoon precipitation over the recent half century. *J. Climate*, **21**, 3833–3852.

Zhou, T. J., L. Zhang, and H. Li, 2008b: Changes in global land monsoon area and total rainfall accumulation over the last half century. *Geophys. Res. Lett.*, **35**, L16707, doi: 10.1029/2008GL034881.